JOURNAL OF AIRCRAFT
Vol. 46, No. 6, November–December 2009

Comparison of Design Methods for Fuel-Cell-Powered Unmanned Aerial Vehicles

Thomas H. Bradley*
Colorado State University, Fort Collins, Colorado 80523-1374
Blake A. Moffitt,† Thomas F. Fuller,‡ and Dimitri N. Mavris§
Georgia Institute of Technology, Atlanta, Georgia 30332-0150
and
David E. Parekh¶
United Technologies Research Center, East Hartford, Connecticut 06108

DOI: 10.2514/1.41658

This paper presents two comparisons of design methods for fuel-cell-powered unmanned aerial vehicles. Previous design studies of fuel-cell-powered aircraft have used design methods that contain intrinsic assumptions regarding the design of a fuel cell powerplant and regarding the interactions between the powerplant and aircraft application. This study seeks to understand the effects of these design assumptions on the fuel cell powerplant structure and the aircraft performance. A design methods comparison is constructed by first developing a multidisciplinary modeling and design environment that is more general than the design processes proposed in literature. The design processes from previous studies can then be imposed on the more complete design environment to determine the performance costs and morphological changes caused by the design assumptions. In the first design study, results show that designing fuel-cell-powered aircraft using automotive-type fuel cell design rules leads to a low-efficiency powerplant and a low-performance aircraft in long-endurance and long-range unmanned aerial vehicle applications. The second design study shows that designing the aircraft powerplant using powerplant design criteria (such as specific energy) rather than aircraft design criteria (such as range) leads to suboptimal aircraft performance, especially for long-endurance unmanned aerial vehicle applications. The results of these studies show that the application-integrated design of aviation-specific fuel cell powerplants can significantly improve the performance of fuel-cell-powered aircraft for a variety of scales and missions.

Nomenclature

A_{FC}	=	fuel cell active area
AR	=	wing aspect ratio
AR_{tank}	=	hydrogen tank length-to-diameter ratio
a	=	penalty function constant
C	=	penalty function constant
d	=	propeller diameter
E_{FC}	=	fuel cell electrical output energy
E_0	=	standard potential of the hydrogen–oxygen reaction
f_{mount}	=	hydrogen tank mounting/bosses/tubing mass fraction
$\mathbf{g}$	=	vector of absolute and side constraints
m_{H2}	=	mass of hydrogen
m_{power}	=	mass of the powerplant, fuel, and hydrogen storage
m_{reg}	=	hydrogen tank regulator mass
n_{cells}	=	number of fuel cells
OEC	=	overall evaluation criteria
P_{FC}	=	fuel cell electrical output power
P_{H2}	=	hydrogen storage pressure
p_{climb}	=	propeller pitch at three-fourths span at climb
p_{cruise}	=	propeller pitch at three-fourths span at cruise
R	=	motor-to-propeller gear ratio
r_{H2}	=	hydrogen tank radius
S_w	=	wing area
$t_{composite}$	=	hydrogen tank composite overwrap thickness
t_{liner}	=	hydrogen tank liner thickness
V_{FC}	=	fuel cell stack potential
X_{motor}	=	electric motor scaling parameter
$\mathbf{x}$	=	vector of design variables
x_{FS}	=	hydrogen tank factor of safety to yield
$\mathbf{x}_{airframe}$	=	vector of airframe design variables
$\mathbf{x}_{power}$	=	vector of hydrogen storage and powerplant design variables
Y_{motor}	=	electric motor scaling parameter
$\mathbf{y}$	=	vector of contributing analysis output variables
ε	=	interior penalty tolerance
ζ	=	penalty function
λ	=	penalty multiplier
ρ_{comp}	=	hydrogen tank composite overwrap density
ρ_{liner}	=	hydrogen tank liner density
$\sigma_{maxcomp}$	=	hydrogen tank composite overwrap maximum stress

Presented as Paper 6413 at the 26th AIAA Applied Aerodynamics Conference,, Honolulu, HI, 18–21 August 2008; received 16 October 2008; revision received 9 June 2009; accepted for publication 19 June 2009.

*Assistant Professor, Department of Mechanical Engineering, Mail Stop 1374. Member AIAA.
†Graduate Student, The Daniel Guggenheim School of Aerospace Engineering, 270 Ferst Drive Northwest. Student Member AIAA.
‡Professor, School of Chemical and Biomolecular Engineering, 311 Ferst Drive Northwest.
§Boeing Professor of Advanced Aerospace Systems Analysis, The Daniel Guggenheim School of Aerospace Engineering, 270 Ferst Drive Northwest. Associate Fellow AIAA.
¶Vice President, Research and Director, 411 Silver Lane, Mail Stop 129-01. Associate Fellow AIAA.

I. Introduction

THE long-endurance unmanned aerial vehicle (UAV) has significant value as a low-cost autonomous reconnaissance and remote-sensing platform for research, commercial, and military missions. Fuel cell powerplants are of interest in this application because of the potential to construct powerplants of high specific energy, low noise, low thermal signature, and improved environmental compatibility.

Because of these performance advantages, fuel cells have recently found their first aviation applications as powerplants for small-scale long-endurance and long-range UAVs. Table 1 lists the demonstrated fuel-cell-powered UAVs known to the authors [1–10]. In 2003, AeroVironment, Inc., a vehicle design and manufacturing company in Monrovia, California, built and flew the first fuel-cell-powered aircraft. Its monopolar polymer electrolyte membrane (PEM) fuel cell system consumes hydrogen from a sodium borohydride reaction vessel. Between those first flights and the present, a number of researchers and commercial entities have developed fuel-cell-powered UAVs of increasing scale and capability. A majority of the demonstration aircraft have used a PEM fuel cell powerplant. A variety of hydrogen storage systems have been used, including gaseous pressure vessels, chemical hydrates, and low-pressure cryogenic liquid hydrogen tanks. A notable technological outlier is the propane-fueled solid-oxide fuel cell (SOFC) UAV that was constructed in 2006 by Advanced Materials, Inc.

The increasing interest in practical fuel-cell-powered UAVs motivated research into appropriate design methods for fuel-cell-powered aircraft. The purposes of these design studies are 1) to characterize the design tradeoffs and optimal configurations of aviation-specific fuel cell powerplants, 2) to compare the performance of fuel cell aircraft to conventional aircraft, and 3) to function as a preliminary design tool in a development process for a fuel cell UAV. Intrinsic to each of these studies is a design process for modeling and selecting the characteristics of the fuel cell UAV powerplants and airframes to be studied. These design processes can be characterized by the scope of their parametric models of the aircraft systems and their definition of design criteria. The three primary design processes for fuel cell powerplants that have been proposed and used in the open literature are described here.

The first proposed design process is based on scaling of a predesigned fuel cell powerplant, as shown in Fig. 1a [11–14]. This scaling method is convenient because it allows aircraft designers to treat the fuel cell powerplant as a monolithic component with characteristics derived from the well-developed automotive fuel cell literature. No detailed fuel cell subsystem or component-level models are required. The scalable fuel cell powerplant model is then combined with a parametric aircraft model and design environment, which can then be optimized for aircraft-level design criteria. This design process is disadvantaged because it cannot model the interactions among the fuel cell components and does not provide low-level information about the proposed fuel cell system to subsequent design and implementation tasks.

The second proposed design process for fuel cell powerplants for aircraft involves designing the fuel cell and its subsystems independently of the design of the aircraft itself, as shown in Fig. 1b [15,16]. Instead of designing the powerplant and aircraft simultaneously toward aircraft-level design criteria (such as range or endurance), the fuel cell powerplant is designed first toward intermediate powerplant-level goals (such as specific energy). The aircraft is then subsequently designed with the now fixed fuel cell powerplant. This process is convenient because it allows the fuel cell aircraft design to be decomposed into independent fuel cell and aircraft design tasks. It also allows for fuel cell powerplant designers to design the detailed specification of the fuel cell powerplant at a component level without considering the aircraft in detail. This method is disadvantaged because it does not take into account the interactions between the fuel cell and aircraft application.

The third proposed fuel cell powerplant design process dispenses with the simplifications proposed by the other methods and attempts to model and design the fuel cell aircraft using a larger design space that includes both the fuel cell subsystem and the aircraft, as shown in Fig. 1c [17,18]. The benefit of this integrated design process is that the interactions between the fuel cell powerplant and the aircraft can be modeled in detail. This allows the design algorithm to simultaneously optimize both the aircraft and the fuel cell subsystems to design fuel cell systems that are specific to the aircraft application, missions, and desired flight characteristics. The disadvantages of this method are associated with the enlarged design space and can include greater design problem complexity and higher computational costs.

Of the three processes reviewed, the third, integrated, design process provides the most design information, but at higher cost than the other methods. This tradeoff between information content and cost is a common one for modelers and designers of complicated systems. If the model or design process is too refined or of too large of scale, then the computational cost becomes too great for use in early stages of design. If the model or design process is computationally efficient but cannot predict the relevant design tradeoffs, then it is of no value for designing among those tradeoffs.

Based on the state of the field, there exists a need to quantify the tradeoffs among the design methods that have been proposed. The goal of this research effort is to determine whether fuel cell aircraft must be designed with the integrated design process (that includes modeling at both the subsystem and application scales) or whether the simplified design processes that have been proposed in literature can maintain acceptable design performance.

This paper presents a design study that provides this comparison among design strategies. First, the integrated modeling and design environment for fuel-cell-powered aircraft is presented. Then the two research tasks associated with this study apply the assumptions associated with the simplified design processes to the integrated process to quantify their differences. Task 1 compares the performance of the integrated fuel cell aircraft design tool to a design tool in which the fuel cell subsystem models and optimizers have been replaced by more conventional automotive-type fuel cell system design rules. Task 2 compares the performance of the integrated design tool with a design tool in which the aircraft models and aircraft-level design criteria (such as endurance or range) have been replaced by powerplant-level design criteria (such as specific energy and specific power). Discussion and conclusions concentrate on the implications of these results on the design and development of fuel-cell-powered UAVs.

II. Integrated Design Environment

Preliminary design synthesis begins with definitions of the systems of interest, the modeling and simulation structure, and the system objectives for evaluation and optimization.

Table 1 Chronological list of published fuel-cell-powered UAV demonstrations

Organization (date), reference	Fuel cell type	Reactant storage type	Endurance (estimated)
AeroVironment, Inc. (2003) [1]	PEM	H_2 sodium borohydride	0.2 h
AeroVironment, Inc. (2005) [2]	PEM	H_2 cryogenic	24 h
Fachhochschule Wiesbaden (2005) [3]	PEM	H_2 gaseous	90 s
Naval Research Laboratory (2006) [4]	PEM	H_2 gaseous	3.3 h
Adaptive Materials, Inc. (2006) [5]	SOFC	Propane	4 h
Georgia Institute of Technology (2006) [6]	PEM	H_2 gaseous	0.75 h
California State University, Los Angeles (2006) [7]	PEM	H_2 gaseous	0.75 h
DLR, German Aerospace Research Center, HyFish (2006) [8]	PEM	H_2 gaseous	0.25 h
California State University, Los Angeles, and Oklahoma State University (2007) [9]	PEM	H_2 gaseous	12 h
Korea Advanced Institute of Science and Technology (2007)[a]	PEM	H_2 sodium borohydride	10 h
AeroVironment, Inc. (2007) [10]	PEM	H_2 sodium borohydride	9 h

[a]Data available online at http://rocket.kaist.ac.kr/03_sub_08.htm [retrieved 10 Aug. 2009].

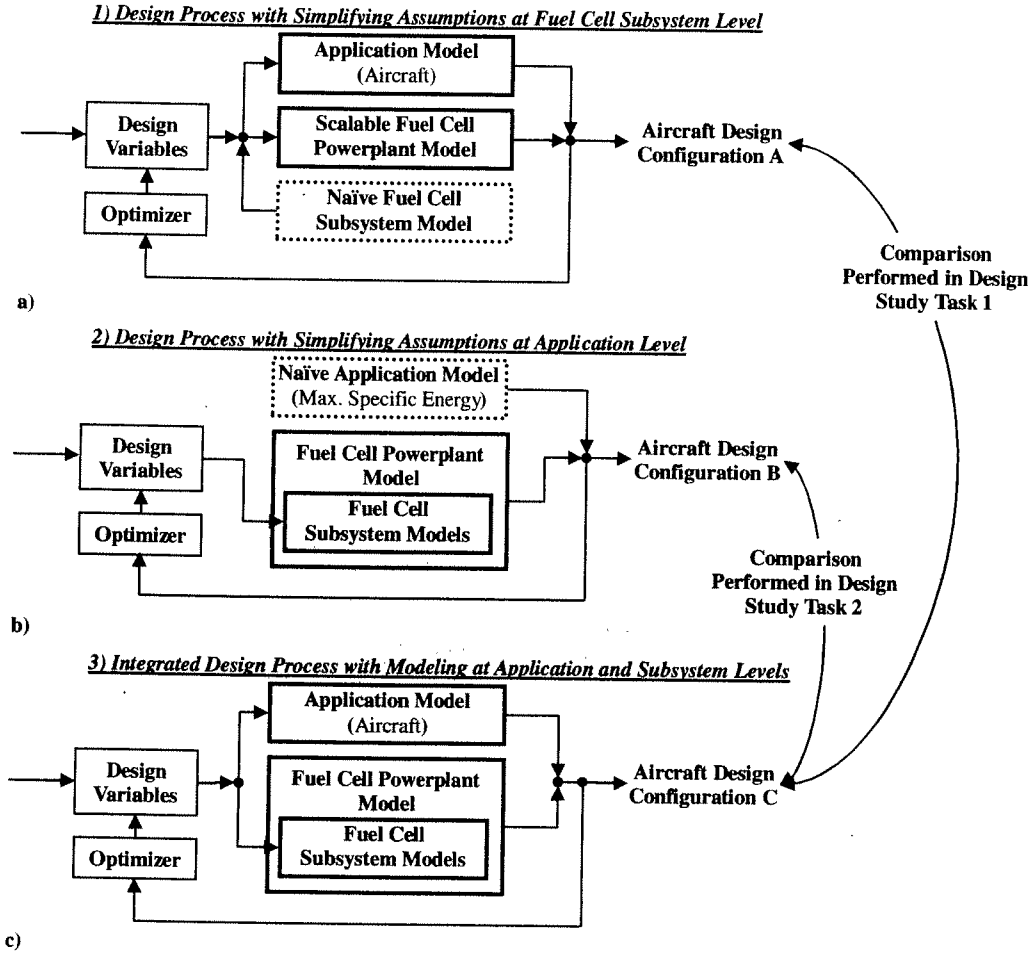

Fig. 1 Comparison of design processes considered in this study.

A. Preliminary Design

This design study takes place at the stage of preliminary aircraft design. The goal of preliminary design is to define the interactions, configuration, layout, dimensions, and performance of the integrated airframe and powerplant system. For this study, we are primarily interested in the synthesis and comparison of near-term-available, small-scale, low-altitude, fuel-cell-powered UAVs that are able to accomplish the generic, low-altitude, long-endurance missions shown in Fig. 2a and the long-range missions shown in Fig. 2b.

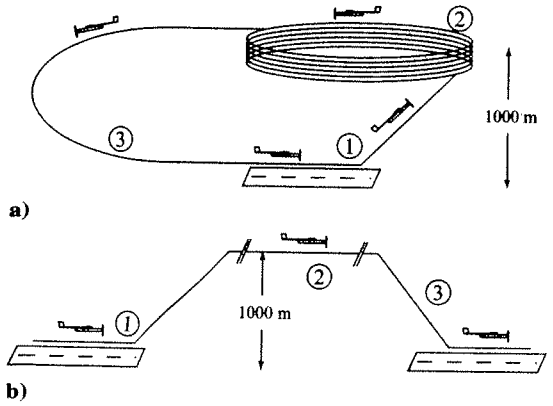

Fig. 2 Example flight paths used for this aircraft design process for a) long-endurance and b) long-range missions broken down into components of 1) takeoff/climb, 2) cruise, and 3) landing.

These restrictions of design scope place requirements and limitations on the models used to represent the performance of the aircraft systems. For instance, the airframe model is designed to be able to model the static performance of highly generic UAVs at low Mach number, at a scale of between 5 and 50 kg of gross takeoff weight. As such, the baseline airframe is a conventional high-wing monoplane, with rear empennage, driven by a tractor propeller. To model the airframe, this study includes parametric model representations of the airframe aerodynamics, structures, mass, stability, geometry, mission segment, payload, and propulsion. Details such as airframe dynamics, rigorous aerodynamic optimization, manufacturability, and costs are left for later stages of design.

The powerplant models are designed to be able to model the steady-state performance of a PEM fuel cell powerplant delivering dc electrical power to a propulsion electric motor and payload. The PEM fuel cell technology is chosen for this study because of its high technology-readiness factor, relatively high specific power, and robustness in mobile applications. To model the powerplant, this study includes parametric model representations of the powerplant, which include models of electrochemical performance, steady-state control, mass, geometry, and component power consumption. Again, low-level implementation challenges are left for later stages of design.

The preliminary design of the aircraft and its powerplant is posed as a canonical multidisciplinary optimization problem. A multidisciplinary analysis (MDA) is used to model the performance of the fuel-cell-powered aircraft as a function of design variables. The MDA is wrapped in an optimization scheme that varies the design variables to reach a deterministic optimum as measured by minimization of a set of design criteria. This deterministic design defines the preliminary design configuration.

B. Powerplant and Aircraft Modeling

To make the analysis of the aircraft tractable, the MDA is decomposed into contributing analyses (CAs). Each CA describes the modeled performance of a single aircraft component as a function of design variables (which are inputs to the multidisciplinary analysis) and as a function of CA variables (which are outputs from other CAs). Thus, to analyze a particular preliminary design, the design variables must be chosen to define the design point in the design space. The MDA is then solved iteratively to reach a converged solution that defines the states of all of the CAs, thereby defining the aircraft performance at that design point.

The CAs presented here are a representative sample of the CAs that comprise the MDA. The design model is described in more detail in [17–19].

1. *Hydrogen Storage Contributing Analyses*

Compressed gaseous hydrogen storage systems are considered for this design study. The compressed hydrogen storage system is modeled as a composite overwrapped pressure vessel using mechanics of materials with design parameters obtained from the literature [20–24], as shown in Table 2. The hydrogen tank is of cylindrical geometry with hemispherical end caps. The tank is subjected only to loading due to the uniform pressure difference between the internal hydrogen pressure and the external atmospheric pressure. In general, composite hydrogen tanks require metallic or polymeric liners to reduce the hydrogen leak rate. The aluminum tank liner is assumed to be of constant thickness and does not contribute to the strength of the tank, but does contribute to its weight. The thickness of the composite overwrap is specified to resist the hoop stress and the axial stress due to the pressure loads. The total composite thickness for the hydrogen tank ($t_{\text{composite}}$) is

$$t_{\text{composite}} = x_{\text{FS}}\left[\frac{r_{\text{H2}}(P_{\text{H2}} - P_{\text{atm}})}{\sigma_{\text{maxcomp}}} + \frac{r_{\text{H2}}(P_{\text{H2}} - P_{\text{atm}})}{2\sigma_{\text{maxcomp}}}\right] \quad (1)$$

and the total tank mass m_{tank} is calculated as the sum of the tank mass, the regulator mass m_{reg}, and the hydrogen mass m_{H2}:

$$m_{\text{tank}} = (1 + f_{\text{mount}}) \cdot (m_{\text{liner}} + m_{\text{composite}}) + m_{\text{reg}} + m_{\text{H2}} \quad (2)$$

The hydrogen tank aspect ratio is constrained to ensure the design of a conventional and commercially available cylinder.

2. *Fuel Cell Contributing Analyses*

Fuel cells are direct electrochemical conversion devices that generate electricity from reactions with atmospheric oxygen and stored hydrogen gas. The fuel cell powerplant is customarily divided into the cell stack assembly and the balance of plant.

The electrochemical characteristics of the fuel cell stack are generally scalable by the number of fuel cells in the cell stack assembly (n_{cells}) and the active area of each cell (A_{FC}). The electrochemical performance of the cell stack is modeled at the single-cell level using a steady-state polarization curve. The stack size and mass scaling factors are based on the characteristics of a prototype stack with 0.48 cm (3/16 in.) graphite bipolar plates, aluminum end plates, and aluminum through-bolts. The performance of the individual fuel cells is equivalent to the published stack performance of the Gore 58 series membrane electrode assembly.** This membrane electrode assembly is chosen as being representative of the state of the art for self-humidified, low-pressure PEM fuel cells. The maximum current density achievable from the fuel cell stack is 1200 mA · cm^{-2} · cell^{-1} and the maximum specific power is 0.6 W · cm^{-2} · cell^{-1}, as shown in Fig. 3.

Table 2 Characteristics of a preliminary compressed hydrogen storage system

Hydrogen storage design parameter	Value	Notes
Composite overwrap maximum stress σ_{maxcomp}	1.9 GPa	Kevlar-49/epoxy at 55% translation [20,21]
Liner density ρ_{linear}	2700 kg · m^{-3}	Aluminum 6061 [22]
Regulator mass m_{reg}	0.35 kg	[6]
Composite overwrap density ρ_{comp}	1530 kg · m^{-3}	[20]
Liner thickness t_{liner}	0.762 mm	Aluminum 6061 [22]
Liner load sharing	0%	[23]
Factor of safety to yield x_{fs}	2.5	—
Tank mounting/bosses/tubing mass fraction f_{mount}	10%	[24]

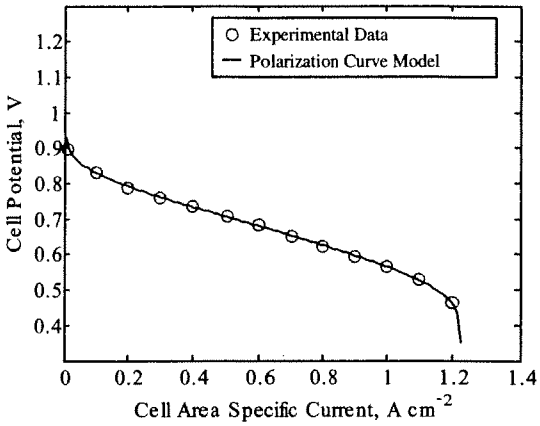

Fig. 3 Fuel cell unit cell performance (see footnote **).

The electrochemical efficiency of the fuel cell system is approximately equal to the ratio of the cell voltage ($V_{\text{FC}}\, n_{\text{cells}}^{-1}$) to the standard potential of the hydrogen–oxygen reaction E_0 [25]:

$$\eta_{\text{FC}} \approx \frac{V_{\text{FC}}}{n_{\text{cells}} E_0} \quad (3)$$

The fuel cell balance of plant represents the air delivery, hydrogen delivery, and regulation, water cooling, and power management and distribution subsystems of the fuel cell. The electrical power consumption and mass of the fuel cell balance of plant are based on the characteristics of previously developed self-humidified low-pressure fuel cell systems. The compressor power consumption and mass are scaled at 1.76 W/liter and 37.75 g/liter of standard air required, values representative of a low-pressure (34 kPa) diaphragm compressor [6]. The water pump consumes 0.05 W of dc electrical power per watt of heat rejected continuously, and the radiator weighs 2.1 g · W^{-1} of fuel cell heat rejected at peak fuel cell power [6].

3. *Airframe Contributing Analyses*

The aerodynamic CA is conducted using both response surface equation (RSE) metamodels and online calculations. Wings2004, a potential flow analysis code, was used to populate an RSE metamodel of induced drag, lift, and interaction effects between the wing and tail [26]. Fuselage lift and drag characteristics and RSE metamodels of the wing induced drag are used to calculate the drag polar of the aircraft using the methods and equations of Roskam [27]. The wing section is a Selig-Donovan 7032 airfoil. Wing aspect ratio is constrained to be less than 20, to realize a conventional and manufacturable wing.

The aircraft empennage section is a NACA 0009 airfoil. Again, Wings2004 is used to derive tail volume coefficient RSEs corresponding to a static margin (scaled by the wing chord) of 20% and an aircraft yawing moment coefficient of 0.15. The empennage is scaled during optimization using these tail volume coefficients.

4. *Propulsion Systems Contributing Analyses*

The electric motor CA is based on a parameterization of a commercially available UAV motor catalog. The electric motor performance is calculated using the manufacturer's recommended

**Data available from W. L. Gore & Associates, Inc.

mathematical model and is parameterized by the motor series number (X_{motor}) and a continuous number related to the number of motor winds (Y_{motor}). Constraints on the values of these design variables keep the motor design within the range of available and manufacturable electric motors. Motor gear ratio is constrained at a maximum reduction of 20 to avoid designing three-stage gear boxes.

The propeller performance CA is based on Goldstein's vortex theory of screw propellers using the Betz condition [28]. The propeller geometries used in this analysis are derived from measurements of several commercially available small-scale propellers. To account for propellers of varying diameter and pitch, the baseline propeller aerodynamic pitch distributions and the planform blade shapes are appropriately scaled while assuming that the airfoil shape distribution along the blade span remains consistent with the baseline propeller. Propeller/fuselage interference is modeled using the method from Lowry [29]. Variable pitch is modeled by allowing the optimizer to determine the optimal propeller pitches for both climbing and cruising flight conditions.

5. *Multidisciplinary Analysis*

These CAs are combined into a MDA, which is shown in design structure matrix form in Table A1 and Fig. A1 in Appendix A. The state of the MDA, $\mathbf{y}$, is controlled by the vector of design variables, $\mathbf{x}$. The design variables and their ranges of validity are presented in Table 3.

C. Design Optimization Methods

Varying the values of the design variables changes the performance of the aircraft model. To design aircraft that can meet the design goals of interest, the MDA is wrapped in an optimization routine that controls the design variables to improve the design of the aircraft by minimizing an overall evaluation criterion (OEC) function, subject to constraints $\mathbf{g}_j(\mathbf{x}, \mathbf{y}(\mathbf{x}))$:

$$\text{Minimize } \text{OEC}(\mathbf{y}(\mathbf{x})) \quad \text{Subject to } \mathbf{0} \le \mathbf{g}_j(\mathbf{x}, \mathbf{y}(\mathbf{x})) \tag{4}$$

A violation of the side constraints can occur when a design variable is outside of the ranges shown in Table 3. Many of the CAs will produce an error if a design variable is outside of the physically feasible ranges (i.e., a hydrogen tank radius of less than 0). In practice, many constrained optimization schemes cannot guarantee that side constraints will not be violated during the solution process. To avoid side-constraint violations, a sequential unconstrained minimization technique (SUMT) was used. The SUMT requires that the objective function to be reformulated as

$$\Phi = \text{OEC}(\mathbf{y}(\mathbf{x})) + \lambda\zeta(\mathbf{x}, \mathbf{y}(\mathbf{x})) \tag{5}$$

Table 3 Design variables and constraints for preliminary design of the fuel cell UAVs in this design study

Design variable	Minimum value	Maximum value
Electric motor scaling parameter X_{motor}	1	12
Electric motor scaling parameter Y_{motor}	0	3
Number of fuel cells n_{cells}	1	∞
Fuel cell active area A_{FC}	1, cm^2	∞, cm^2
Hydrogen tank radius r_{H2}	0, m	∞, m
Hydrogen tank length-to-diameter ratio AR_{tank}	1	4
Hydrogen storage pressure P_{H2}	0, MPa	∞, MPa
Propeller diameter d	0, m	∞, m
Wing area S_w	0, m^2	∞, m^2
Wing aspect ratio	1	20
Propeller pitch at three-fourths span at cruise p_{cruise}	0, m	∞, m
Propeller pitch at three-fourths span at climb p_{climb}	0, m	∞, m
Motor-to-propeller gear ratio R	0.1	20

The parameter λ is a scalar multiplier and $\zeta(\mathbf{x}, \mathbf{y}(\mathbf{x}))$ is a scalar penalty function dependent on the design variables $\mathbf{x}$ and the CA output variables $\mathbf{y}$. To force the optimization procedure to favor feasible designs and to avoid possible discontinuities caused by the introduction of the penalty function, $\zeta(\mathbf{x}, \mathbf{y}(\mathbf{x}))$ is defined using an interior penalty method:

$$\zeta(\mathbf{x}, \mathbf{y}(\mathbf{x})) = \sum_{j=1}^{n} \mathbf{g}_j(\mathbf{x}, \mathbf{y}(\mathbf{x})) \tag{6}$$

The vector $\mathbf{g}_j$ represents the absolute and side constraints, and n is the total number of absolute and side constraints. The vector $\mathbf{g}_j$ and the interior penalty tolerance $\varepsilon = -C \cdot (\lambda)^a$ are defined so that when the design point is far from violating the constraints,

$$\mathbf{g}_j(\mathbf{x}) > \varepsilon \quad \text{and} \quad \mathbf{g}_j(\mathbf{x}, \mathbf{y}(\mathbf{x})) = -\frac{2\varepsilon - \mathbf{g}_j(\mathbf{x}, \mathbf{y}(\mathbf{x}))}{\varepsilon^2} \tag{7}$$

As the design point approaches the constraints,

$$\mathbf{g}_j(\mathbf{x}, \mathbf{y}(\mathbf{x})) \le \varepsilon \quad \text{and} \quad \mathbf{g}_j(\mathbf{x}, \mathbf{y}(\mathbf{x})) = -\frac{1}{\mathbf{g}_j(\mathbf{x}, \mathbf{y}(\mathbf{x}))} \tag{8}$$

The scalar values of $C = 0.246$ and $a = 0.417$ were used in all calculations based on preference weighting of the design criteria [30]. For the first stage of the optimization, $\lambda = 0.006$ was used. The converged solution of the first-stage optimization provides the starting point for the next optimization stage. For the next stage λ is decreased to 10% of its previous value and the optimization routine is repeated using the previous solution as a starting point. This is continued until the acceptable convergence criteria have been met.

For all studies, the Nelder–Mead algorithm is used as implemented in MATLAB 6.1. The Nelder–Mead algorithm shows robust convergence and computational efficiency, taking approximately 1500 iterations and a 4 h per design process using an Intel P4 duo 2.2 GHz personal computer.

III. Task 1: Comparison of Powerplant Design Rules

The goal of task 1 is to compare the performance of a fuel cell aircraft design that uses a scalable fuel cell powerplant model and conventional fuel cell subsystem assumptions (aircraft design configuration A in Fig. 1) with an aircraft design that allows fuel cell subsystem models to interact and become optimized (aircraft design configuration C in Fig. 1).

When fuel cell aircraft design studies have used scalable fuel cell powerplant models with conventional fuel cell subsystem assumptions, they have inherited the scaling factors and design assumptions from the automotive fuel cell literature. For instance, the design process used in many fuel cell system design studies assumes that the air supply compressor is sized by the active-area-limited current of the fuel cell. This assumption states that the maximum airflow of the air supply compressor is proportional to the amount of air that the fuel cell stack requires to produce its peak (i.e., active-area-limited) current and that the air supply rate should not be the limiting factor in developing peak fuel cell power [12,31]. This assumption is relevant for fuel-cell-powered automobiles in which the performance of the automobile is highly dependent on the stack output power [32], but its relevance for the low-power, high-energy design space associated with fuel cell UAVs is unknown.

We can use the tools developed for this study to understand the intrinsic limitations in this conventional design process and to determine what more optimal balance-of-plant design rules might be for long-endurance and long-range fuel-cell-powered aircraft. To emulate the fuel cell aircraft design studies that use scaled automotive fuel cell information to design fuel cell aircraft, an automotive-type fuel cell balance-of-plant sizing routine will be imposed on the integrated design environment described in Sec. II.

A. Design Study Methods

To conduct this comparison, we will design two fuel-cell-powered aircraft using two different design processes. The differences

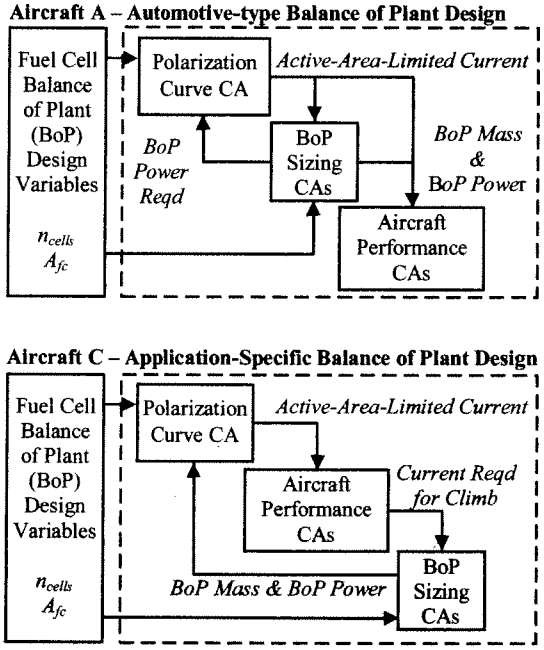

Fig. 4 Design structure comparison between two fuel cell system design rules.

between these design processes are shown conceptually in Fig. 4. Figure 4 shows the portion of the MDA in which the fuel cell and balance of plant are analyzed. Both aircraft have the same design variables (fuel cell active area and number of fuel cells) input to this portion of the MDA, and both aircraft use the same CAs or groups of CAs (polarization curve CA, balance-of-plant sizing CAs, and aircraft performance CAs). The difference between the design method for aircraft A and aircraft C is in the structure of the MDA and the inputs to the balance-of-plant sizing CA.

Aircraft A is designed with the automotive-type design assumption that the balance of plant is sized as a function of the active-area-limited current. In aircraft A, the output of the balance-of-plant sizing CA is passed forward to the aircraft performance CA to be sure that balance-of-plant mass and power requirements are taken into account in the aircraft performance calculation. An output of the balance-of-plant sizing CA is also passed backward to the polarization curve CA iteratively to ensure that the current coming from the fuel cell represents both the current required by the aircraft and the current required by the fuel cell balance of plant. The inputs to the balance-of-plant sizing CA are the number of fuel cells and the active-area-limited current.

Aircraft C is designed so that the balance of plant is sized by the actual current required of the aircraft during climb. For the balance-of-plant sizing CA to have that information accessible, the aircraft performance CA must have already been run. This requirement means that the aircraft performance code must be within the feedback loop between the polarization curve and balance-of-plant sizing CAs.

The conventional design rules used to design aircraft A have a number of preliminary and computational benefits. Conceptually, aircraft A is a simpler aircraft to compartmentalize for design. Whereas aircraft A has weak links between the fuel cell CAs and the aircraft performance CAs, aircraft C has feedbacks between the fuel cell design tasks and the aircraft design tasks. This structure makes the design structure matrix computationally more expensive to evaluate and converge. The design process for aircraft A is also easier to partition into discrete and disciplinary fuel cell analysis tasks and aircraft performance analysis tasks.

(An analogy to a more familiar technology can improve the conceptual understanding of the differences between these design strategies. We will describe two methods for sizing the radiator of a car. The first method assumes that the radiator must be sized to reject the heat output of the engine while running on an engine test stand at 100% throttle ad infinitum. The second method assumes that the radiator must be sized for the real-world worst-case requirements of the car, perhaps a fully loaded drive up the continent's steepest road at full speed. The first design process is easier to compartmentalize during design, as the radiator sizing is completely independent of the vehicle design. No modeling of vehicle loads, roads, wind, and ambient temperature is required. The second design process requires these models to be part of the design process but reaches a lighter-weight, lower-cost solution that is adequate for all feasible conditions. The first radiator design process is analogous to the balance-of-plant design process for aircraft A, and the second radiator design process is analogous to the balance-of-plant design process for aircraft C.)

This design experiment is repeated for both range and endurance and at a variety of constrained aircraft weights. Task 1 of this design study does not include a mechanism for studying the computational efficiency of the design processes. Because the design assumptions to be studied are imposed on the existing design environment, the computational performances of the processes are not rigorously optimized for computation time.

B. Results

Aircraft A and aircraft C are then designed to maximize on-station endurance, subject to a 125 m/min climb-rate constraint and a maximum weight constraint of 30 kg. The design characteristics of the two aircraft are shown in Table 4 and Fig. 5. Comparing the performance of the two aircraft shows that aircraft C is a longer-endurance, and therefore more optimal, aircraft than aircraft A. This suggests that the integrated balance-of-plant design is more effective than the conventional design assumptions. Figures 5 and 6 provide some insight into the design tradeoffs that the optimizer is exploiting to improve the performance of aircraft C. Figure 5 compares the subsystem weight breakdown for the two aircraft designs. Figure 6 shows the fuel cell stack polarization curves for the two aircraft designs. Three points per curve are indicated in Fig. 6. The condition of the fuel cell is shown at the cruise and climb condition for each aircraft. Figure 6 also shows the active-area-limited current, which represents the maximum current that the fuel cell stack could produce, given an unconstrained reactant flow.

Based on Eq. (9), the dual goals of the design optimization tool are to minimize the objective function and to satisfy the constraints. Although both the objective function (endurance) and many of the constraints (climb rate) are aircraft-level metrics, these objectives force requirements of power and energy on the fuel cell powerplant. To meet the climb constraint, the optimization algorithm must add electrical output power to the fuel cell system by adding additional fuel cell active area or an additional number of fuel cells. To add additional endurance, the optimizer must increase the mass of fuel stored on the aircraft by shrinking the fuel cell and balance-of-plant mass, or it must improve the fuel conversion efficiency of the

Table 4 Comparison of aircraft characteristics for aircraft A and aircraft C

Aircraft characteristics	Aircraft A automotive-type BoP design	Aircraft C application-specific BoP design
On-station endurance, h	26.5	33.6
Hydrogen tank volume, liter	16.0	19.8
Number of fuel cells	69	58
Fuel cell active area, cm^2	31.4	48.1
Fuel cell mass, kg	21.1	21.0
Fuel cell output power at cruise, W	333.0	330.1
Aircraft climb rate, m/min	125.3	125.3
Fuel cell output power at climb, W	1218	1249

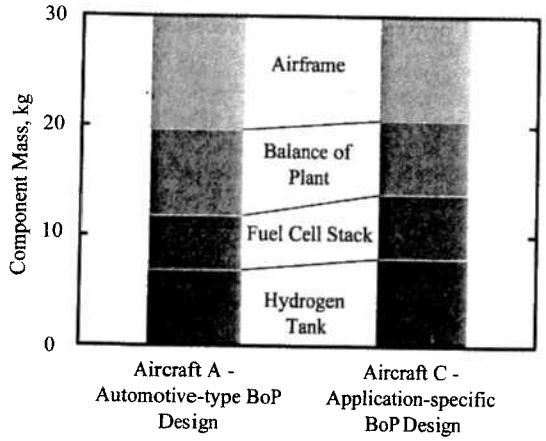

Fig. 5 Mass breakdown among major subsystems for comparison between conventional and integrated balance-of-plant design.

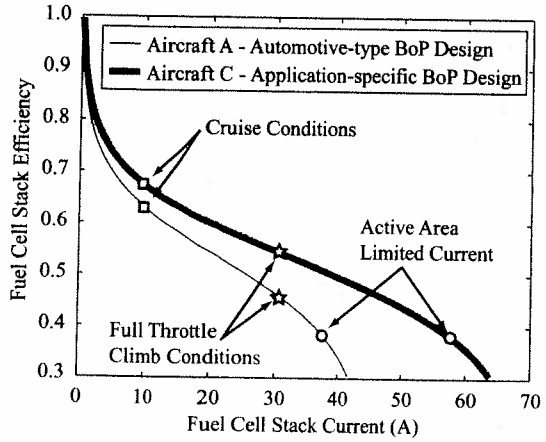

Fig. 6 Fuel cell stack efficiency at various operating conditions for comparison between conventional and integrated balance-of-plant design.

powerplant by adding fuel cell active area or an additional number of fuel cells to reduce the fuel cell current loading.

For aircraft A, the optimizer handles the dueling requirements by designing a fuel cell with a relatively small active area and a larger number of cells. The design rules for aircraft A demand that the balance of plant be scaled by the active-area-limited current. To avoid a very weighty balance of plant, the optimizer keeps the fuel cell active area small. This is shown in Fig. 7 by the small peak current for aircraft A and the close proximity of the climb-condition operating point to the active-area-limited current point. Despite the small size of aircraft A's fuel cell stack, Fig. 5 shows that the balance of plant for aircraft A is still more massive than the balance of plant for aircraft C.

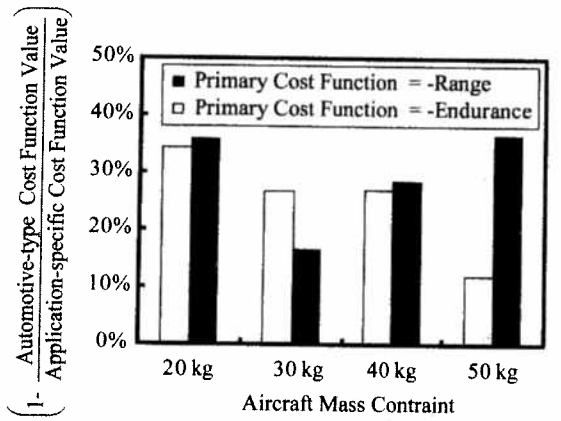

Fig. 7 Design of experiment results for comparison between conventional and integrated balance-of-plant design. The ordinate defines the percentage improvement in the primary cost function achieved using the application-specific balance-of-plant design process.

For aircraft C, the design of the fuel cell balance of plant is decoupled from the scaling of the fuel cell, and the optimizer is able to discover a more optimal configuration. Figure 6 shows that because of this decoupling, the current required by the aircraft at climb is roughly half of the active-area-limited current. In other words, the fuel cell stack is roughly two times larger than is necessary to meet the power demands of the aircraft. This suggests that the optimizer is moving toward a larger fuel cell stack to reduce its current density, thereby improving its efficiency, as defined in Eq. (3). Because the balance-of-plant sizing and fuel cell active area are decoupled, the balance of plant can be undersized for the fuel cell stack, reducing its weight, while still allowing it to manage the fuel cell for all realizable performance conditions. Of course, increasing the fuel cell size makes it more massive relative to the fuel cell specified for aircraft A, but this mass difference is made up for by the decreased mass of the balance of plant.

Results for the design of experiments with varying design criteria and maximum aircraft weight constraints are shown in Fig. 7. In all cases tested there is a marked performance improvement using the integrated design balance-of-plant design rules relative to the automotive-type design rules. This performance improvement is robust to changes in the design criteria and scale of the aircraft.

IV. Task 2: Comparison of Powerplant Design Criteria

The goal of task 2 of this design study is to compare the performance of fuel cell aircraft powerplants that are designed without considering the detail requirements of the aircraft application (aircraft design configuration B in Fig. 1) with powerplants that are designed using an application-integrated modeling and design process (aircraft design configuration C in Fig. 1).

Many design studies for fuel-cell-powered aircraft have used powerplant specific energy as a surrogate design criterion for designing long-endurance fuel cell powerplants. Powerplant specific energy is the ratio of the electrical output energy of the fuel cell (E_{FC}) to the mass of the powerplant, fuel, and hydrogen storage (m_{power}). Replacing the application-level design criterion of endurance with the powerplant-level design criterion of specific energy allows for a simplification and compartmentalization of the powerplant design process. The assumption of equivalence between these criteria can been justified by assuming that the powerplant and fuel mass is a large fraction of the aircraft mass and by assuming that aircraft specific energy $E_{FC}\, m_{power}^{-1}$ is closely related to the quantity $E_{FC}\, m_{power}^{-3/2}$. $E_{FC}\, m_{power}^{-3/2}$ is directly proportional to aircraft endurance for aircraft cruising under conditions of constant velocity, mass, lift, and drag [33,34]. Perhaps obviously, design toward system optima will produce better system designs than design toward subsystem optima, but the degree of compromise is unclear. As in task 1, we can use the tools developed for this study to determine to what degree these surrogate design criteria reduce the effectiveness of the design process and under what applications their assumptions break down.

A. Design Study Methods

The design tools developed for this study allow for the generalized comparison between a design optimized for subsystem performance metrics (such as $E_{FC}\, m_{power}^{-1}$, $E_{FC}\, m_{power}^{-3/2}$, and $P_{FC}\, m_{power}^{-1}$) and a design optimized for aircraft-level performance metrics (such as endurance, range, and climb rate). This comparison will be made by designing fuel-cell-powered aircraft for both aircraft-level and powerplant-level design criteria and by making comparisons between the performance of the resulting aircraft. A final step of the design study determines whether the aircraft optimal performance can be recovered through manipulation of the aircraft design once the powerplant design variables are frozen at the powerplant-level optimum.

The experimental method for this design study is described here. The aircraft is designed for maximum range at a maximum aircraft

weight of 40 kg and a minimum climb rate of 125 m/min. The procedure is generalized in Table 5 for a long-range aircraft and in Table 6 for a long-endurance aircraft.

Let the vector of design variables, $\mathbf{x}$, be split into a set of design variables that control the powerplant and hydrogen storage design ($\mathbf{x}_{\text{power}}$) and a set of design variables that control the airframe design ($\mathbf{x}_{\text{airframe}}$).

$$\mathbf{x} = [\mathbf{x}^T_{\text{power}} \quad : \quad \mathbf{x}^T_{\text{airframe}}]^T \tag{9}$$

$$\mathbf{x}^T_{\text{power}} = [n_{\text{cells}} \quad A_{\text{FC}} \quad r_{\text{H2}} \quad \text{AR}_{\text{tank}} \quad P_{\text{H2}}] \tag{10}$$

$$\mathbf{x}^T_{\text{airframe}} = [X_{\text{motor}} \quad Y_{\text{motor}} \quad \text{AR} \quad d \quad S_w \quad p_{\text{cruise}} \quad p_{\text{climb}} \quad R] \tag{11}$$

1) The aircraft is first designed for maximum range, using all design variables, subject to side constraints of a 125 m/min climb-rate constraint and a maximum mass constraint of 40 kg. This step ensures that the subsequent design steps occur in the neighborhood of a feasible point in the design space. This configuration also serves as the experimental control. Optimization toward design criteria other than maximum range will move away from this aircraft-level optimized design configuration.

2) From this baseline, the powerplant is then redesigned for maximum powerplant specific energy $E_{\text{FC}}\, m^{-1}_{\text{power}}$ using only the powerplant and hydrogen storage design variables ($\mathbf{x}_{\text{power}}$). The aircraft-level side constraint on climb rate is replaced with a single powerplant-level side constraint on specific power $P_{\text{FC}}\, m_{\text{power}}$. This step allows the optimizer to seek out a subsystem optimum in terms of powerplant design metrics at fixed specific power. This step approximates the action of a naïve designer, designing a fuel cell aircraft powerplant to maximize specific energy while maintaining a fixed specific power.

3) The powerplant design is then fixed and the aircraft is designed using only the airframe design variables $\mathbf{x}_{\text{airframe}}$. Again, the aircraft is designed for maximum range subject to side constraints: a 125 m/min climb-rate constraint and a maximum mass constraint of 40 kg. This step approximates the action of an aircraft designer who is given a fixed powerplant design and must maximize performance using only aircraft design variables.

A similar procedure for conducting the same study using aircraft-level design criteria of endurance and the powerplant-level design criteria of $E_{\text{FC}}\, m^{-3/2}_{\text{power}}$ is shown in Table 6. These procedures are repeated for a design of experiments with variable cost functions and aircraft mass constraints. Similar to task 1, task 2 does not include a mechanism for studying the computational efficiency of the design processes. Because the design assumptions functionally split the aircraft design into powerplant and airframe design steps, the computational performances of the processes are not rigorously comparable.

B. Results

Figure 8 shows the trajectory of a range-optimal design study as it progresses. The steps of the study are broken down into individual subplots with arrows showing the progress of the optimization routine. The study begins at the lower left corner of Fig. 8a, which has axes of aircraft range and $E_{\text{FC}}\, m^{-1}_{\text{power}}$. As the first optimization progresses, the aircraft configuration improves in terms of both range and $E_{\text{FC}}\, m^{-1}_{\text{power}}$. The optimizer reaches a range-optimal solution, with all constraints met at point 1. Although configurations with higher range are explored by the design optimization scheme, these configurations do not meet the design constraints and are therefore not optimal with respect to Eq. (9). Step 2 of the design study starts at point 1, as shown in Fig. 8b. The design study now begins to optimize the fuel cell powerplant for the powerplant-level metric of $E_{\text{FC}}\, m^{-1}_{\text{power}}$, regardless of its effect on the aircraft-level metric of endurance. As the $E_{\text{FC}}\, m^{-1}_{\text{power}}$ of the aircraft powerplant increases, the range of the aircraft decreases. At point 2, the optimization algorithm finds the configuration with the highest available $E_{\text{FC}}\, m^{-1}_{\text{power}}$ and with all powerplant-level constraints met. Step 3 of the design study begins from point 2 and attempts to improve the range of the aircraft and meet aircraft-level performance constraints using only the aircraft design variables. This step is shown in Fig. 8c. In practice, the optimizer is unable to significantly improve the range while still meeting the climb-rate constraint.

Step 1 of the design process has derived the optimal configuration for the aircraft-level design metrics and aircraft-level constraints. From Fig. 8a, we can see that for these fuel cell aircraft, aircraft range is roughly proportional to the powerplant performance metric of $E\, m^{-1}_{\text{power}}$. A similar relationship exists between endurance and the quantity $E_{\text{FC}}\, m^{-3/2}_{\text{power}}$. It is this proportionality that provides the justification for using $E_{\text{FC}}\, m^{-1}_{\text{power}}$ and $E_{\text{FC}}\, m^{-3/2}_{\text{power}}$ as surrogates for aircraft range and endurance.

Steps 2 and 3 of the design process allows us to compare the effectiveness of integrated aircraft/powerplant design and disintegrated powerplant and aircraft design that uses subsystem-level design metrics with guide powerplant design. A comparison of design point 1 with design point 3 shows that design of fuel cell aircraft using the powerplant-level performance metrics of $E_{\text{FC}}\, m^{-1}_{\text{power}}$ and $P_{\text{FC}}\, m^{-1}_{\text{power}}$, are a poor substitute for an aircraft-integrated design process. The range of the $E_{\text{FC}}\, m^{-1}_{\text{power}}$ optimized aircraft is 6.6% less than the optimum when aircraft weight is constrained at 40 kg.

These experiments are repeated for both range and endurance and at a variety of constrained aircraft weights. Results are shown in Fig. 9. In each case tested, the aircraft-level design criteria produce improved results relative to the powerplant-level design criteria. For the range-optimal aircraft, the difference between the

Table 5 Tabular summary of steps associated with the range design metric comparison experiment

	Step 1: aircraft design configuration C	Step 2	Step 3: aircraft design configuration B
Goal	Initialize design at aircraft optimum	Move toward fuel cell optimum	Move back toward aircraft optimum
Cost function	Range	$E_{\text{FC}}\, m^{-1}_{\text{power}}$	Range
Constrained variables	Climb rate	$P_{\text{FC}}\, m^{-1}_{\text{power}}$	Climb rate
Active design variables (DVs)	Fuel cell and aircraft DVs $\mathbf{x}$	Fuel cell and aircraft DVs $\mathbf{x}$	Airframe DVs $\mathbf{x}_{\text{airframe}}$

Table 6 Tabular summary of steps associated with the endurance design metric comparison experiment

	Step 1: aircraft design configuration C	Step 2	Step 3: aircraft design configuration B
Goal	Initialize design at aircraft optimum	Move toward fuel cell optimum	Move back toward aircraft optimum
Cost function	Endurance	$E_{\text{FC}}\, m^{-3/2}_{\text{power}}$	Endurance
Constrained variables	Climb rate	$P_{\text{FC}}\, m^{-1}_{\text{power}}$	Climb rate
Active design variables (DVs)	Fuel cell and aircraft DVs $\mathbf{x}$	Fuel cell and aircraft DVs $\mathbf{x}$	Airframe DVs $\mathbf{x}_{\text{airframe}}$

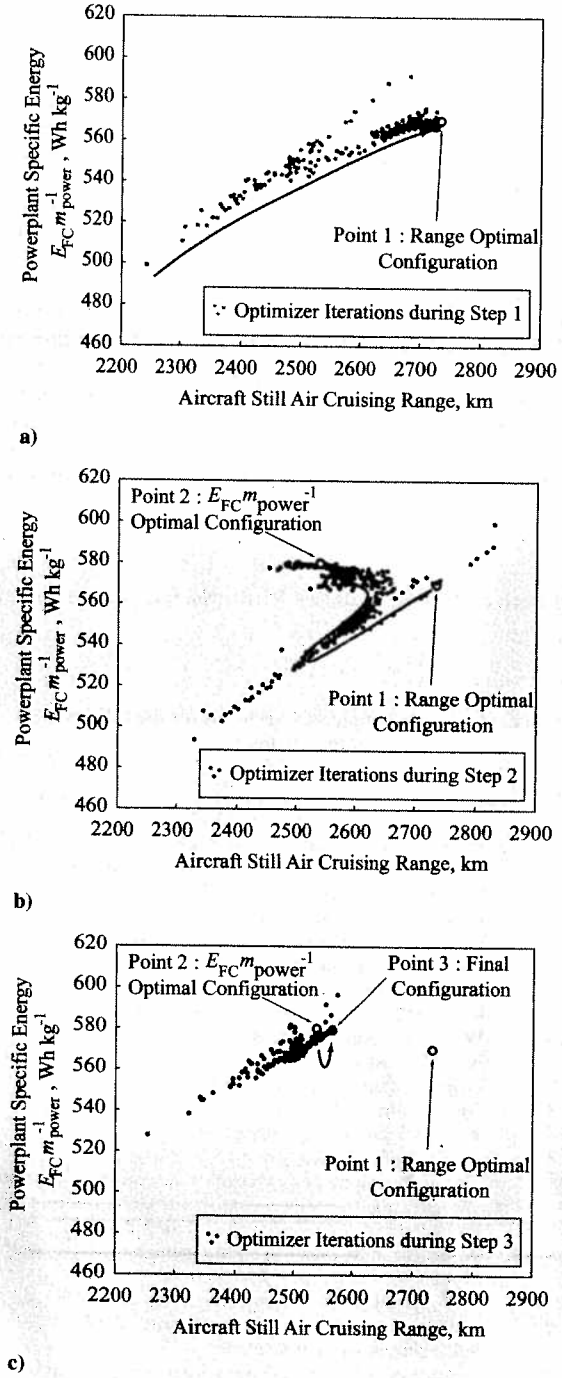

Fig. 8 Breakdown of steps associated with range-optimal design study at aircraft mass = 40 kg: a) step 1, b) step 2, and c) step 3.

subsystem-optimized results and the system-optimized results decreases with increasing aircraft mass. This occurs because as the aircraft weight grows, the ratio of powerplant to aircraft weight increases. This improves the validity of the assumptions required to equate specific energy and range. For endurance-optimal aircraft, the opposite relation is present. The larger the aircraft, the less effective the powerplant-level design criteria of $E_{FC}\, m_{power}^{-3/2}$ is at emulating the effects of the application-level design criteria of endurance.

V. Discussion

The results of the two tasks performed for this design study show that the design assumptions that have been proposed in literature are substantially less effective at defining optimal aircraft configurations than a design process that allows for powerplant design at both powerplant subsystem and application levels. By enlarging the

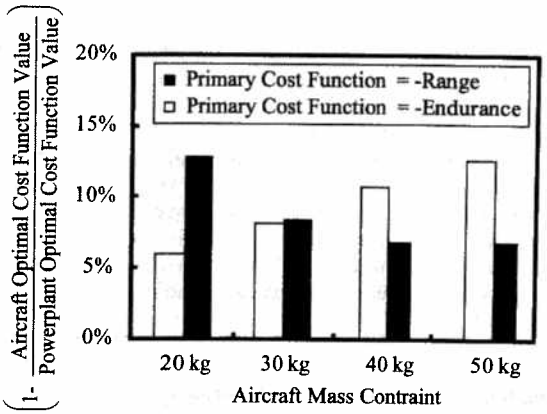

Fig. 9 Design of experiment results for design metric comparison study with percentage improvement from aircraft-level design metric optimization. The ordinate defines the percentage improvement in the primary cost function achieved using aircraft-level design metrics.

design space in this manner, the integrated design environment allows for the concurrent design of fuel cell systems *and* aircraft systems that are specific to the fuel-cell-powered aircraft application.

As stated in the Introduction, the purposes of the fuel cell aircraft design studies that have been performed to date are 1) to characterize the design tradeoffs and optimal configurations of aviation-specific fuel cell powerplants, 2) to compare the performance of fuel cell aircraft to conventional aircraft, and 3) to function as a preliminary design tool in a development process for a fuel cell UAV. Based on the results of the two design study tasks, the relative performance of the three design processes can now be discussed, referencing these intended purposes.

A. Implications for Characterization of Aviation-Specific Fuel Cell Powerplants

Based on the generalized results of these studies, the integrated design process can begin to define the characteristics of fuel cell powerplants for aircraft and the characteristics of the airframe for long-endurance and long-range fuel-cell-powered aircraft.

In terms of the system-level fuel cell powerplant characteristics, fuel cell powerplants for UAV applications are characterized by high specific energy (although this characteristic is indicative, not predictive, of high performance as explored in detail in task 2). The mechanical specific energy of the powerplants designed for these studies shows specific energies of up to 600 dc (W · h)/kg. Although this is more than double the specific energy of automotive fuel cell systems, the specific power of UAV fuel cell systems designed for this study is up to four times lower than is required for automotive applications [35]. These results suggest that the technological requirements for fuel-cell-powered UAVs are quite different from those of automotive application. High-energy, low-power, energy storage technologies such as solid-oxide or direct-methanol fuel cells may be able to find an early niche in fuel-cell-powered UAVs.

At the level of the fuel cell subsystems, there are sizing and morphological changes relative to more conventional fuel cell applications. Whereas automotive design studies have shown that the fuel cell balance of plant should be sized to approximately 80–90% of the active-area-limited power [32], this study suggests that 45–50% is more optimal for long-endurance and long-range fuel cell aircraft. For another example, automotive hydrogen storage systems have continued to progress toward higher storage pressure [36]. In the UAV application, a pressure near 30 MPa appears to be a broad optimum. Continued exploration of the fuel cell UAV design space is necessary before these rules can be extended beyond the technologies, scales, and missions considered in this study.

B. Implications for Comparisons of Fuel-Cell-Powered and Conventional Aircraft

The improved results that are available using the integrated aircraft design process also have implications for interpretation of fuel cell

aircraft design studies that have been performed to date. Studies have shown that there exist certain scales and missions in which the performance of fuel-cell-powered UAVs in long-endurance or long-range missions can surpass the performance of conventional internal combustion and battery-powered UAVs [1,16,34]. The performance improvement that can be realized from advanced design techniques expands the regions of the design space in which fuel cell powerplants for aircraft can outperform more conventional powerplants. The substantial improvements in fuel cell aircraft endurance (up to 37%) that are shown in this study may have a large effect on the results of the technology comparison studies that exist in the literature [14].

C. Implications for Fuel Cell UAV Preliminary Design

The results detailed in this study have relevance for the developers of real-world fuel-cell-powered aircraft. Preliminary design has an important role to play in the design process of a new system, such as a fuel cell powerplant. Preliminary design establishes the relevant connections among subsystems, the limits of the design space, and the performance tradeoffs among options. Imposing design assumptions on the preliminary design process compromises these functions and reduces the design freedom that is available during early stages of design. Instead, by increasing the size of the design space and reducing the design assumptions embedded in preliminary design, lower-performing designs can be down-selected through the multidisciplinary optimization process rather than through assumptions. In general, this leads to improved design performance and more robust decision-making [37]. By eliminating the conventional design rules that have constrained fuel cell aircraft design to date, the integrated design process detailed in this study shows improved optimality relative to the state of the art. In addition, because the integrated design process models the fuel cell system at the fuel cell subsystem level, there is an improved level of design detail available for use in later stages of design. Integration of preliminary and detail design is also improved because the integrated design process models the fuel cell system at the component level, mimicking the component specification process that is commonly used in the detailed development of fuel cell systems.

VI. Conclusions

This paper has presented a method for multidisciplinary design and optimization of fuel-cell-powered UAVs. The design tools developed as a component of this research effort allow for the comparison of the effectiveness of the fuel cell powerplant design methods that have been used in literature.

The first task of this study compares the fuel cell powerplants of aircraft designs that incorporate automotive-type balance-of-plant sizing rules to those in which the design rules are derived via multidisciplinary optimization. Task 1 showed that for all of the aircraft studied, using fuel cell balance-of-plant design rules derived from multidisciplinary optimization resulted in a 12–37% improvement in design aircraft performance. Results show that the UAV application places unique requirements on the fuel cell system that makes the optimal fuel cell system design different from conventional automotive-type fuel cell systems. The integrated design of the fuel cell, balance of plant, hydrogen storage, powertrain, and airframe allows for the assessment of design tradeoffs among these components.

The second task of this study compares an integrated aircraft/powerplant design method to a disintegrated powerplant and aircraft design method that uses powerplant-level design metrics to guide powerplant design. When compared with optimization toward preestablished powertrain performance metrics such as $E_{FC}\ m_{power}^{-1}$, $E_{FC}\ m_{power}^{-3/2}$, or $P_{FC}\ m_{power}^{-1}$, the use of application-level design criteria allows for substantial improvement in the on-design performance of the aircraft. Improvements in the aircraft design criteria of range and endurance varied between a negligible 6% and a more substantial 13%.

Of the literature regarding the structure, performance, control, and design of fuel cell systems, the vast majority is specific to automotive and stationary applications. The design of fuel cell systems for aviation applications will require new design rules that may be in opposition to convention. This study shows that the design processes that have been used in the design and technological assessments of fuel-cell-powered aircraft exhibit considerable design disadvantages relative to design processes that allow for application-integrated design of fuel cell systems at a powerplant subsystem level. Future work will assess the sensitivity of these designs to offdesign conditions and design parameter uncertainties.

There are a number of potential fuel cell applications that might benefit from the advanced design techniques applied in this work. Underwater unmanned vehicles, automobiles, spacecraft, and mobile power supplies are just some of the applications in which fuel cell powerplant design and control will be strongly constrained by requirements of the application. In these cases, application-integrated powerplant design will result in improved performance.

Appendix A: Details of the Multidisciplinary Analysis

Table A1 Contributing analysis labels for the MDA design structure matrix

CA number	Description
1	Motor mass and dimensions calculation
2	Fuel cell dimensions and mass calculation
3	Hydrogen tank mass and dimensions calculation
4	Hydrogen storage capacity calculation
5	Hydrogen mass conversion
6	Hydrogen storage system mass calculation
7	Propeller and motor mass sum
8	Fuel cell system mass sum
9	Fuselage mass and dimensions calculation
10	Wing and tail mass calculation
11	Aircraft mass sum
12	Propeller interference calculation
13	Fuselage drag calculation
14	Wing and tail lift drag calculation
15	Airplane lift and drag sum
16	Steady level flight power demand calculation during climb
17	Propeller nondimensional number calculation during climb
18	Propeller coefficients calculation during climb
19	Propeller torque calculation during climb
20	Motor speed calculation during climb
21	Fuel cell polarization calculation during climb
22	Auxiliary current load calculation during climb
23	Stack current sum during climb
24	Balance-of-plant power consumption during climb
25	Electrical power summation during climb
26	Electrical system efficiency calculation during climb
27	Propeller nondimensional number calculation
28	Propeller coefficients calculation
29	Propeller thrust calculation
30	Propeller torque calculation during climb
31	Motor current calculation
32	Fuel cell polarization calculation
33	Auxiliary current load calculation
34	Stack current sum during climb
35	Balance-of-plant power consumption
36	Electrical power summation
37	Electrical system efficiency calculation
28	Climb-rate calculation
39	Propeller tip Mach number constraint analysis
40	Reynolds number constraint analysis
41	Hydrogen flow rate calculation
42	Hydrogen flow rate calculation during climb
43	Mission endurance calculation
44	Mission range calculation
45	Overall evaluation criteria calculation

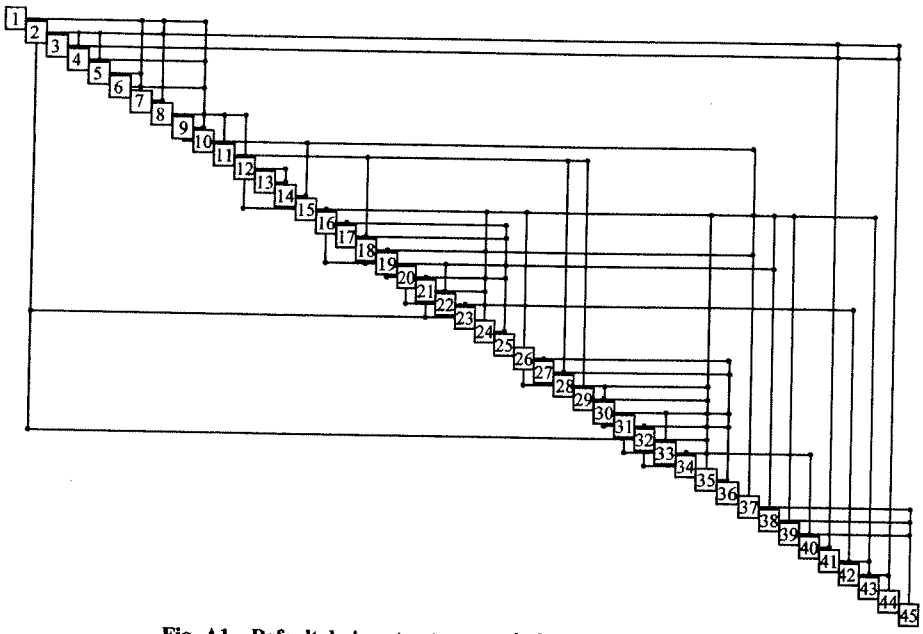

Fig. A1 Default design structure matrix for fuel cell UAV design.

Acknowledgments

This research was funded in part by the NASA University Research Engineering Technology Institute (URETI) grant to the Georgia Institute of Technology. The authors would also like to thank the many research engineers at the Georgia Tech Research Institute and the Aerospace Systems Design Laboratory who provided valuable expertise and guidance over the course of the project.

References

[1] Velev, O., "Summary of Fuel Cell Projects: AeroVironment 1997–2007," *National Hydrogen Association Fall 2007 Topical Forum*, Columbia, SC, Oct. 2007.

[2] "Aerovironment Flies World's First Liquid Hydrogen-Powered UAV," AeroVironment, Inc., Monrovia, CA, June 2005.

[3] Scheppat, B., "Betriebsanleitung fur das BrennstoffZellenbetriebene Modellflugzeug," Fachhochschule Wiesbaden, Wiesbaden, Germany, 2004.

[4] Kellogg, J., "Fuel Cells for Micro Air Vehicles," *Joint Service Power Exposition*, Tampa, FL, May 2005.

[5] Crumm, A., "Solid Oxide Fuel Cell Systems," *Proceedings of the Fuel Cell Seminar*, Honolulu, HI, Nov. 2006.

[6] Bradley, T. H., Moffitt, B., Mavris, D., and Parekh, D. E., "Development and Experimental Characterization of a Fuel Cell Powered Aircraft," *Journal of Power Sources*, Vol. 171, No. 2, 2007, pp. 793–801. doi:10.1016/j.jpowsour.2007.06.215.

[7] "Cal State L.A.'s Fuel-Cell Plane Passes Key Flight Test," California State Univ., Los Angeles, Los Angeles, Sept. 2006.

[8] Anon., "Erfolgreicher Erstflug des Hyfish," DLR, German Aerospace Center, Stuttgart, Germany, 3 April 2007.

[9] Herwerth, C., Chiang, C., Ko, A., Matsuyama, S., Choi, S. B., Mirmirani, M., Gamble, D., Arena, A., Koschany, A., Gu, G., and Wankewycz, T., "Development of a Small Long Endurance Hybrid PEM Fuel Cell Powered UAV," Society of Automotive Engineers Paper 2007-01-3930, Sept. 2007.

[10] McConnell, V. P., "Military UAVs Claiming the Skies with Fuel Cell Power," *Fuel Cells Bulletin*, Vol. 2007, No. 12, Dec. 2007, pp. 12–15. doi:10.1016/S1464-2859(07)70438-8

[11] Friend, M. G., and Daggett, D. L., "Fuel Cell Demonstrator Airplane," AIAA Paper 2003-2868, July 2003.

[12] Kohout, L. L., and Schmitz, P. C., "Fuel Cell Propulsion Systems for an All-Electric Personal Air Vehicle," AIAA Paper 2003-2867, July 2003.

[13] Baldock, N., and Mokhtarzadeh-Dehghan, M. R., "A Study of Solar-Powered, High-Altitude Unmanned Aerial Vehicles," *Aircraft Engineering and Aerospace Technology*, Vol. 78, No. 3, 2006, pp. 187–193.

[14] Nickol, C. L., Guynn, M. D., Kohout, L. L., and Ozoroski, T. A., "High Altitude Long Endurance Air Vehicle Analysis of Alternatives and Technology Requirements Development," AIAA Paper 2007-1050, Jan. 2007.

[15] Burke, K. A., "Unitized Regenerative Fuel Cell Development," NASA TM-2003-212739, 2003.

[16] Himansu, A., Freeh, J. E., Steffen, C. J., Tornabene, R. T., and Wang, X.-Y.J., "Hybrid Solid Oxide Fuel Cell/Gas Turbine System Design for High Altitude Long Endurance Aerospace Missions," NASA TM-2006-214328, 2006.

[17] Moffitt, B. A., Bradley, T. H., Parekh, D. E., and Mavris, D. N., "Design Space Exploration of Small-Scale PEM Fuel Cell Unmanned Aerial Vehicle," AIAA Paper 2006-7701, Sept. 2006.

[18] Moffitt, B., Bradley, T. H., Mavris, D., and Parekh, D. E., "Reducing Design Error of a Fuel Cell UAV through Variable Fidelity Optimization," AIAA Paper 2007-7793, Sept. 2007.

[19] Bradley, T. H., Moffitt, B. A., Mavris, D. N., and Parekh, D. E., "Validated Modeling and Synthesis of a Medium-scale Polymer Electrolyte Membrane Fuel Cell Aircraft," 4th International ASME Conference on Fuel Cell Science, Engineering and Technology, American Society of Mechanical Engineers, Paper 2006-97233, June 2006.

[20] Colozza, A. J., "Hydrogen Storage for Aircraft Applications Overview," NASA CR-2002-211867, 2002.

[21] Lark, R. F., "Recent Advances in Lightweight, Filament-Wound Composite Pressure Vessel Technology," *Energy Technology Conference*, Houston, TX, Sept. 1977.

[22] Shigley, J., Mischke, C., and Budynas, R., *Mechanical Engineering Design*, 7th ed., McGraw–Hill, New York, 2003.

[23] Kawahara, G., and McCleskey, S. F., "Titanium-Lined, Carbon Composite Overwrapped Pressure Vessel," AIAA Paper 1996-2751, July 1996.

[24] Harris, J., Grande, R., and Higgins, M., "Ultralight Propellant Tank for NASA Space Technology 5," AIAA Paper 2003-4608, July 2003.

[25] Larminie, J., and Dicks, A., *Fuel Cell Systems Explained*, 2nd ed., Wiley, Hoboken, NJ, 2003.

[26] Phillips, W. F., and Snyder, D. O., "Modern Adaptation of Prandtl's Classic Lifting-Line Theory," *Journal of Aircraft*, Vol. 37, No. 4, 2000, pp. 662–670. doi:10.2514/2.2649

[27] Roskam, J., *Airplane Design Part 6: Preliminary Calculation of Aerodynamic, Thrust and Power Characteristics*, DAR Corp., Lawrence, KS, 2000.

[28] Goldstein, S., "On the Vortex Theory of Screw Propellers," *Proceedings of the Royal Society of London, Series A: Mathematical and Physical Sciences*, Vol. 123, No. 792, 1929, pp. 440–495. doi:10.1098/rspa.1929.0078

[29] Lowry, J. T., *Performance of Light Aircraft*, AIAA Education Series, AIAA, Reston, VA, 1999.

[30] Vanderplaats, G. N., *Numerical Optimization Techniques for Engineering Design*, McGraw–Hill, New York, 1984.
[31] Gelfi, S., Stefanopoulou, A. G., Pukrushpan, J. T., and Peng, H., "Dynamics of Low-Pressure and High-Pressure Fuel Cell Air Supply Systems," *American Control Conference*, American Automatic Control Council, Evanston, IL, June 2003, pp. 2049–2054.
[32] Kim, M.-J., and Peng, H., "Power Management and Design Optimization of Fuel Cell/Battery Hybrid Vehicles," *Journal of Power Sources*, Vol. 165, No. 2, 2007, pp. 819–832. doi:10.1016/j.jpowsour.2006.12.038
[33] Phillips, W. F., *Mechanics of Flight*, Wiley, Hoboken, NJ, 2004.
[34] Bradley, T. H., Moffitt, B.A., Mavris, D. N., and Parekh, D. E., "Fuel Cells for Aviation Applications," *Encyclopedia of Electrochemical Power Sources*, Elsevier, Amsterdam, 2009.
[35] Friedlmeier, G., Friedrich, J., and Panik, F., "Test Experiences with the Daimler Chrysler Fuel Cell Electric Vehicle NECAR 4," *Fuel Cells*, Vol. 1, No. 2, 2001, pp. 92–96. doi:10.1002/1615-6854(200107)1:2<92::AID-FUCE92>3.0.CO;2-I
[36] Deluchi, M., "Hydrogen Vehicles: An Evaluation of Fuel Storage, Performance, Safety, Environmental Impacts, and Cost," *International Journal of Hydrogen Energy*, Vol. 14, No. 2, 1989, pp. 81–130. doi:10.1016/0360-3199(89)90001-3
[37] Mavris, D. N., DeLaurentis, D. A., Bandte, O., and Hale, M. A., "A Stochastic Approach to Multi-Disciplinary Aircraft Analysis and Design," AIAA Paper 98-0912, Jan. 1998.